
Smooth Deep Saliency

Rudolf Herdt^{1,2} Maximilian Schmidt^{1,2} Daniel Otero Bager^{1,2} Peter Maaß¹

Abstract

In this work, we investigate methods to reduce the noise in deep saliency maps coming from convolutional downsampling, with the purpose of explaining how a deep learning model detects tumors in scanned histological tissue samples. Those methods make the investigated models more interpretable for gradient-based saliency maps, computed in hidden layers. We test our approach on different models trained for image classification on ImageNet1K, and models trained for tumor detection on Camelyon16 and in-house real-world digital pathology scans of stained tissue samples. Our results show that the checkerboard noise in the gradient gets reduced, resulting in smoother and therefore easier to interpret saliency maps.

1. Introduction

For critical applications, such as in the healthcare sector, it is important to gain an insight into how the model arrives at its decision. To gain such an understanding, saliency methods can be used, ideally highlighting the structures on which the model relies to support its prediction. Saliency methods are usually applied at either the input or the last convolutional layer (Selvaraju et al., 2017). Their application in the input layer leads to noisy results, and in the final convolution layer, the saliency map lacks detail. In this paper, we focus on the middle ground and apply saliency methods in hidden layers. This gives us smoother results while preserving the details. As a result, we can use high-quality saliency maps to identify individual cell nuclei, which are used by trained models to detect tumors. On the one hand, using hidden layers also allows us to observe the transition from lower-level features, like the outline of cell nuclei in a Resnet18 (He et al., 2016) trained on Camelyon16 (Ehteshami Bejnordi et al., 2017) data or individual cell nuclei for a segmentation model trained on digital pathology (Digipath) data at a lower magnification, highlighted in earlier layers. On the

other hand, it also gives access to higher-level features in deeper layers, e.g. segmenting the whole cell nuclei for the Resnet18 model or structures formed by cells for the model trained on Digipath data.

A problem in computing gradient-based saliency maps in hidden layers of a model that uses convolutional downsampling is the checkerboard noise this downsampling introduces to its gradient, similar to what transposed convolutions exhibit in the forward pass (Odena et al., 2016). This noise dominates the resulting saliency map and makes them very difficult to interpret. Therefore, in this paper, we investigate several methods to remove that checkerboard noise, which allows us to use saliency methods in hidden layers and test them on several models and datasets.

With a stride 2 convolution (downsampling), not every input pixel gets multiplied by every weight. Due to the stride of 2, every other pixel is skipped, which can introduce a checkerboard pattern with a periodicity of 2 in the gradient (see Section 2.1). Since that noise is coming from the convolutional downsampling, we can mitigate it by changing the backward pass of each convolutional downsampling layer, in order to let each input pixel receive a gradient by each weight. The other method we use is to train a bilinear surrogate model, where we replace each convolutional downsampling with a bilinear downsampling combined with two trainable stride 1 convolutions, one before and after the bilinear downsampling. These are then trained to match the behavior of the original model. That way, we can compare the accuracy and predictions of the surrogate model to the original model (by only changing the backward pass of the convolutional layer, but we no longer know whether we still explain the original model). The output of each surrogate path, consisting of the two stride 1 convolutions with the bilinear downsampling in between, should match the output of the convolutional downsampling it replaces concerning the L1 loss. We train this bilinear surrogate model on the training data of the original model. We show that the accuracy and predictions of the surrogate model closely match those of the original model, while the generated saliency maps have less noise, as measured by total variation.

¹Center for Industrial Mathematics, University of Bremen
²aisencia. Correspondence to: Rudolf Herdt <rherdt@uni-bremen.de>.

2. Related Work

Saliency maps are used to highlight structures in the input that the model utilized for its prediction. The saliency methods could be divided into three groups. First, those that only utilize activations like CAM (Oquab et al., 2015), secondly those that also utilize gradients of backpropagation like Grad-CAM (Selvaraju et al., 2017), DeepLift (Shrikumar et al., 2019), Integrated Gradients (Sundararajan et al., 2017), or simply using the gradient (Simonyan et al., 2014). And lastly perturbation base methods like RISE (Petsiuk et al., 2018), which are usually applied at the input. Perturbation-based methods generally require several evaluations of the model, which makes them slow. To get gradient-based methods more stable SmoothGrad (Smilkov et al., 2017) can be employed, which runs the saliency method several times each time adding Gaussian noise to the input and then returning the average saliency map.

Gradient-based saliency methods are usually applied at either the input layer or the last convolutional layer, like (Selvaraju et al., 2017), whereas we focus on computing the saliency maps from hidden layers of the model. (Olah et al., 2018) also computes saliency maps at hidden layers and couples them with feature visualization. To mitigate noise in the saliency maps, they employ Gaussian blurring. (Rao et al., 2022) also used Gaussian blurring to smooth saliency maps of hidden layers. We limit ourselves to models that utilize convolutional downsampling and, instead of using Gaussian blurring, we work on removing the source of the noise.

(Olah et al., 2017) visualized neurons of a CNN, and observed that the visualizations become more high-level the deeper the neuron is located in the model. We observe something similar in the attribution for the Camelyon16 and Digipath models, where in earlier layers the cell nuclei are outlined and in deeper layers segmented (Camelyon16). And the saliency map for the Digipath model highlights individual cell nuclei in earlier layers and structures formed by them in deeper layers.

2.1. Checkerboard Noise from Stride 2 Convolution

With a stride 2 convolution, not every pixel is multiplied by every weight. Due to the stride of 2, every other pixel is skipped. As an example, let x be a matrix of ones with a size of 16×16 , $k = \begin{pmatrix} 1 & 1 \\ 1 & -1 \end{pmatrix}$ and $*$ the operator for a stride 2 convolution. Figure 1 shows the result of calculating $\nabla_x(\sum x * k)$, i.e. the gradient towards x when computing the sum of the convolution of x with kernel k . We can see a periodic checkerboard pattern in the gradient. The black pixels were multiplied by -1.0 from the kernel and, therefore, received a gradient of -1.0 . In contrast, the white pixels were multiplied by the 1.0 value from the kernel and

received a gradient of 1.0 . That is the noise pattern we mitigate with our methods.

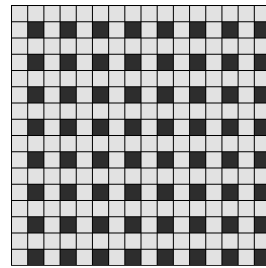


Figure 1. Checkerboard pattern in the gradient of the 16×16 image.

3. Methods

In this section, we show an overview of our bilinear surrogate method. In addition, we describe the evaluation metrics we use and how we compute the saliency maps.

3.1. Overview

To reduce the checkerboard noise in the gradient coming from the convolutional downsampling, we investigate three different methods:

- **Bilinear Surrogate:** Replacing each convolutional downsampling with a bilinear surrogate path (consisting of two stride 1 convolutions with a bilinear downsampling in between them), as shown in Figure 2. This approach requires training data, in order to train the surrogate paths.
- **Backward Hook:** Changing the backward pass of each convolutional downsampling, by taking the gradients it would normally propagate backward, rolling them 4 times spatially, and returning the mean of those 4 tensors. We roll them by (h, w) pixels with h and w being $(0, 0)$, $(0, 1)$, $(1, 0)$, $(1, 1)$. The rolling means that the line of pixels that would be shifted outside of the image, moves to the opposite side of the tensor.
- **Forward Hook:** Changing the forward pass of each convolutional downsampling in a way that we get the gradients of the second method by default. This means we run the forward pass 4 times, each time with a spatially rolled input, and return the mean of those 4 tensors. We roll them the same as in the method mentioned directly above, namely by $(0, 0)$, $(0, 1)$, $(1, 0)$, $(1, 1)$ pixels. Although changing only the backward pass as described in the method above is enough to remove the checkerboard noise, changing the forward pass allows us to compare the accuracy and predictions against the original model.

With the bilinear surrogate approach, all convolutional downsamplings except the first one in the model are replaced. Similarly, with the forward and backward hook approach, we do not change the behavior of the first convolutional downsampling. We do not replace the first one, since we always compute the saliency maps towards a deeper layer, therefore we do not need to replace it.

In training of the bilinear surrogate model, we replace each convolutional downsampling individually (i.e. we only use the convolutional downsampling in the forward pass and not the bilinear surrogate one). But in the evaluation, we use them all together, as visible from Figure 3. We use the L1 loss as a loss function in training.

3.2. Evaluation

With our bilinear surrogate method, we aim to achieve two goals:

- Reduce the checkerboard noise in the gradient to make saliency maps in hidden layers more interpretable.
- Match the accuracy of the original model. Because the idea would be to use the bilinear surrogate model instead of the original model. Therefore, the accuracy needs to be as good as the original model.

To validate whether we succeeded in reducing the checkerboard noise in the gradient, we can visually inspect some saliency maps. Further, we also run total variation (TV) on the saliency maps over a validation dataset. To evaluate how well we match the prediction behavior of the original model, we compare the accuracy and/or difference in prediction for only the target class and all classes of the original and the surrogate model on a validation dataset. For the difference in prediction, we use the output of the model after softmax. Then we compute the difference in prediction twice: Once only for the target class and once for all classes. For only the target class that would be: Let \tilde{y} the prediction of the original model and \hat{y} be the prediction of the bilinear surrogate model and c be the target class, then the difference in prediction would be: $|\tilde{y}_c - \hat{y}_c|$. Whereas for all classes we would do: $\sum_c |\tilde{y}_c - \hat{y}_c|$, where we compute the sum over all classes.

For the segmentation model on the Digipath data, we often have more than one class per image. Therefore, we compute the difference in prediction for the target class differently. For each sample, we only consider the non-background label with the majority of pixels. If the whole target is background, we skip that sample. Then, from the target and the original prediction, we build a binary mask. In that binary mask, we set a pixel to 1 if the original prediction (which is after softmax) for the target label at that pixel is larger than 0.1. Otherwise, we set the pixel value to 0. Finally, we report

the weighted L1 loss between the prediction of the original model and the surrogate model (respectively the prediction of the forward hooked model), based on the mask, i.e. let M be the binary mask, then we do $(\sum_c |\tilde{y}_c - \hat{y}_c|) \cdot \frac{1}{\sum M}$

3.3. Computing the Saliency Map

We use two methods to compute the saliency maps. One is DeepLift, with a black image (zeros) as the baseline. The other is simply computing the gradient. We combine both with SmoothGrad, where we use 20 samples and Gaussian noise with a standard deviation of $\sigma = 0.2$ as values for the parameters. The saliency map is computed using the logits output of the model (before softmax or sigmoid). Let f be a function (in our case either DeepLift or gradient) that takes the image and baseline and returns the saliency map, x the image and b the baseline and $z^{(i)} \sim \mathcal{N}(0, 0.2)$. With SmoothGrad we compute the mean $\frac{1}{n} \sum_{i=1}^n f(x + z^{(i)})$, with $n = 20$ in our case.

For image classification, we compute the saliency map against the ground truth label. For semantic segmentation, if we only have the background class as a label, we compute the saliency map against the background label. Otherwise, we compute it against the majority non-background label.

3.4. Total Variation

In this section, we describe how we compute the total variation (TV) to measure the noise in the saliency maps. To evaluate how much noise our methods remove, we compute the TV of the saliency map from the original model and the surrogate model and compare the values. Since we only want to measure the noise and not the scale of it, we first process the saliency map before measuring TV. Let z be the saliency map, then for each channel z_c separately, we first set the mean to zero,

$$z'_c = z_c - \mu(z_c) \quad (1)$$

and then divide by the mean of the absolute value and compute the mean over the channels (with n being the number of channels)

$$\sum_c \frac{1}{n} \text{TV}\left(\frac{z'_c}{\max(\mu(|z'_c|), \epsilon)}\right) \quad (2)$$

ϵ is set to 10^{-6} and is used to avoid division by zero (i.e. if z'_c is zero everywhere). Equation (2) is the resulting total variation reported in the experiments section.

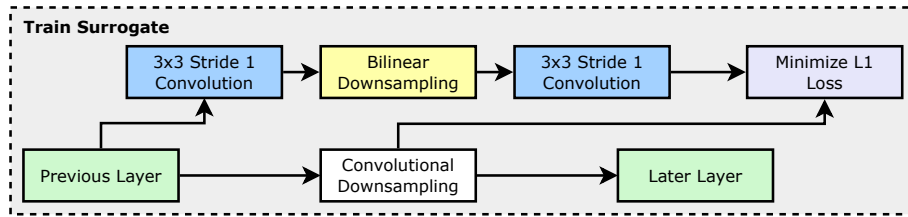


Figure 2. Training the bilinear surrogate. The weights of the two 3×3 stride 1 convolutions are not shared, they are different convolutions.

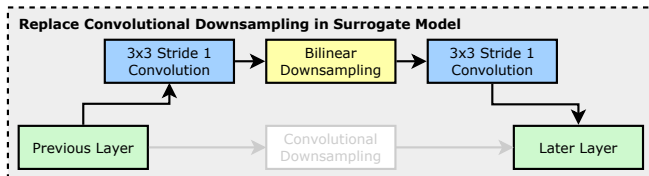


Figure 3. Using the bilinear surrogate path in evaluation. The convolutional downsamplings will be ignored, they are replaced by the bilinear surrogate.

4. Experiments

4.1. Setup

In this section we describe the hardware, datasets and models we use in our experiments.

4.1.1. HARDWARE AND SOFTWARE

For all our experiments, we use a Linux server with 8 Nvidia RTX 2080 Ti GPUs. On the software side, we use PyTorch (Paszke et al., 2019) version 1.13.1 with CUDA version 11.6 and torchvision version 0.14.1. For computing the saliency maps we use the Captum library (Kokhlikyan et al., 2020) version 0.6.0.

4.1.2. TRAINING

In this paragraph we describe the training setup we use in order to train the bilinear surrogate model. The forward and backward hook approaches work on the original model, and require no additional training. All networks in our experiments are running in eval mode. We only train the bilinear surrogate paths, each consisting of two 3×3 stride 1 convolutions, with a bilinear downsampling in between them. The rest of the network is kept frozen. On the ImageNet1K (Deng et al., 2009) and Digipath data we train the bilinear surrogate for 10 epochs, and on the Camelyon16 data we train it for 2 epochs, as shown in Table 1. As optimizer we use Adam (Kingma & Ba, 2015) with a learning rate of 0.001. As batch size we use 64 for training the surrogate models on the ImageNet1K data, 512 for the Camelyon16 data (due to class imbalance between tumor and no tumor we use a larger batch size here) and 16 for the Digipath data

Table 1. Train- and validation set sizes for the three datasets ImageNet1K, Camelyon16, and Digipath.

| | IMAGENET1K | CAMELYON16 | DIGIPATH |
|-----------------------|------------|------------|-----------|
| TRAINING SAMPLES | 1 281 167 | 99 410 615 | 129 634 |
| VALIDATION SAMPLES | 50 000 | 50 000 | 899 |
| TV VALIDATION SAMPLES | 500 | 500 | 899 |
| USED IMAGE SIZE | 224x224 | 224x224 | 1536x1536 |
| TRAINING EPOCHS | 10 | 2 | 10 |

Table 2. Accuracy on the ImageNet1K validation data.

| NETWORK | ORIGINAL ACCURACY | SURROGATE ACCURACY | FORWARD HOOK ACCURACY |
|-----------------|-------------------|--------------------|-----------------------|
| RESNET34 | 73.29 | 73.12 | 53.25 |
| RESNET50 | 76.15 | 76.05 | 73.00 |
| RESNET50 ROBUST | 57.89 | 57.86 | 56.10 |

(due to the larger patch size of 1536 we use a smaller batch size here).

4.1.3. DATASETS

We evaluate our method on three datasets:

- **ImageNet1K.** We evaluate the accuracy and the difference in prediction between the original and surrogate model on the 50 000 validation images. The total variation is evaluated on every hundredth image of the validation data, resulting in 500 images.
- **Camelyon16.** The difference in prediction is evaluated on all the 46 267 899 validation samples. The total variation is evaluated on 500 samples randomly chosen out of the validation samples.
- **Digipath.** This is an in-house dataset which is not openly available. Here the training data consists of 129 634 images. We evaluate the difference in prediction and total variation on 899 images not used in training of the original or surrogate model.

4.1.4. MODELS

On the ImageNet1K data we use a ResNet34 and a ResNet50 both openly available from the pytorch model zoo. Further,

Table 3. Prediction difference between original and bilinear surrogate model, measured after softmax.

| NETWORK | BILINEAR SURROGATE | | FORWARD HOOK | |
|---------------------|-------------------------|------------------------|-------------------|-------------------|
| | ALL CLASSES | ONLY TARGET CLASS | ALL CLASSES | ONLY TARGET CLASS |
| RESNET34 | 9.52 \pm 12.31 | 2.39 \pm 4.08 | 95.84 \pm 66.84 | 30.26 \pm 31.33 |
| RESNET50 | 8.90 \pm 12.48 | 2.38 \pm 4.25 | 39.44 \pm 45.58 | 11.38 \pm 17.30 |
| RESNET50 ROBUST | 5.84 \pm 4.37 | 0.97 \pm 1.39 | 38.55 \pm 25.62 | 7.95 \pm 10.52 |
| RESNET18 CAMELYON16 | 0.40 \pm 1.41 | 0.40 \pm 1.41 | 3.63 \pm 10.40 | 3.63 \pm 10.40 |
| RESNET34 DIGIPATH | 4.05 \pm 2.11 | 2.04 \pm 1.09 | 37.33 \pm 34.36 | 19.76 \pm 16.15 |

we use an adversarially robust ResNet50 from (Santurkar et al., 2019). For the Camelyon16 data we use an openly available ResNet18 from the monai model zoo. And for the Digipath data we use an in-house U-Net segmentation model with a ResNet34 backbone.

4.2. Results

In this section we describe the results of our experiments. First we show the accuracy of the original model, the surrogate model and the forward hook approach, as well as the difference in prediction compared to the original model.

4.2.1. ACCURACY AND PREDICTION DIFFERENCE

Table 2 shows the accuracy of the original, bilinear surrogate and forward hooked models, on the ImageNet1K data. For the bilinear surrogate models we observe a maximum decrease of accuracy of 0.17 for the ResNet34 model, and a minimum decrease of 0.03 for the robust ResNet50 model. The forward hooked models have a larger decrease of accuracy, especially in the case of the ResNet34 model where the accuracy decreases by 20.04.

In Table 3 we evaluate how the prediction of the models changes, once for the sum over all predicted classes and once only for the target class. We report the differences in softmax values times 100 (i.e. a reported difference of 9.52 for ResNet34 would mean a difference of 0.0952). The first three models (ResNet34, ResNet50 and ResNet50 Robust) are originally trained on ImageNet1K, as are the surrogate models. Consequently, we evaluate the difference in prediction for them on the ImageNet1K validation data. The ResNet18 Camelyon16 model and surrogate model are trained on Camelyon16, therefore we evaluate on the validation data of Camelyon16. And the ResNet34 Digipath model and surrogate model are trained on the in-house Digipath dataset, and evaluated on data not seen in training. For the bilinear surrogate models we observe the maximum change of prediction for the sum of all classes and only for the target class of 9.52 respectively 2.39 for the Resnet34 model. That aligns with the drop of accuracy being largest for the ResNet34 surrogate model. We observe the smallest change in prediction of 0.40 for the ResNet18 Camelyon16 model. Since we only have a single class there, the result for 'all classes' and 'only target class' is the same. In the case

of the forward hooked models, the predictions differ more strongly. Here the largest change in prediction of 95.84 for the sum over all classes and 30.26 for only the target class is again in the ResNet34 model. The smallest change is 3.63 also again for the ResNet18 Camelyon16 model. Overall the bilinear surrogates match the accuracy and prediction of the original models much closer compared to the forward hooked models.

4.2.2. TOTAL VARIATION

Table 4 shows the total variation (TV) of the saliency map for both the original and surrogate models, both for DeepLift and Gradient. We report the mean and standard deviation over the validation data. The results have some stochasticity since we add gaussian noise to the input (we use SmoothGrad where we run the saliency method 20 times each time adding gaussian noise with a standard deviation of 0.2 to the input, and return the mean of those 20 runs as the saliency map). Layer1, Layer2 and Layer3 denote the last layer at that resolution stage. This means Layer1 is the last layer where the input has been downsampled twice, Layer2 is the last layer where it has been downsampled three times, and Layer3 is the last layer where it has been downsampled four times. We use two saliency methods: DeepLift and Gradient (which is simply the gradient with respect to the hidden layer).

With our bilinear surrogate models, we observe a reduction of TV of the saliency map compared to the original model, through all models and layers. For DeepLift we observe an average reduction in TV of 21.6%, with a minimum of 9.6% in Layer3 of ResNet50 trained on ImageNet1K, and a maximum of 47.8% in Layer3 of ResNet34 trained on Digipath. Even greater reductions can be observed with the Gradient method. There we observe an average reduction in TV of 31.5%, with a minimum of 18.2% in Layer3 of ResNet50 trained on ImageNet1K, and a maximum of 58.0% in Layer3 of ResNet34 trained on Digipath.

Figure 4 shows the total variation for the original and bilinear surrogate model for the ResNet34, ResNet50 and ResNet50 Robust models on ImageNet1K when computing the saliency map using the Gradient method. TV is shown on the y-axis, whereas the layer is on the x-axis. The figure shows the total variation for all the layer blocks starting

Table 4. Total variation of the saliency map

| NETWORK | LAYER | DEEPLIFT | | | | GRADIENT | | | |
|---------------------|--------|---------------|--------------------|---------------|----------------------|---------------|--------------------|----------------------|----------------------|
| | | ORIGINAL | BILINEAR SURROGATE | BACKWARD HOOK | FORWARD HOOK | ORIGINAL | BILINEAR SURROGATE | BACKWARD HOOK | FORWARD HOOK |
| RESNET34 | LAYER1 | 2.711 ± 0.059 | 2.110 ± 0.096 | 1.858 ± 0.114 | 1.824 ± 0.117 | 2.627 ± 0.025 | 1.846 ± 0.052 | 1.301 ± 0.047 | 1.335 ± 0.044 |
| | LAYER2 | 2.132 ± 0.066 | 1.860 ± 0.089 | 1.751 ± 0.098 | 1.678 ± 0.085 | 1.713 ± 0.039 | 1.285 ± 0.058 | 0.990 ± 0.047 | 0.968 ± 0.041 |
| | LAYER3 | 2.165 ± 0.049 | 1.879 ± 0.062 | 1.775 ± 0.071 | 1.693 ± 0.061 | 1.894 ± 0.051 | 1.326 ± 0.048 | 1.054 ± 0.038 | 1.025 ± 0.036 |
| RESNET50 | LAYER1 | 2.774 ± 0.055 | 2.156 ± 0.090 | 1.777 ± 0.110 | 1.757 ± 0.105 | 2.660 ± 0.030 | 1.986 ± 0.060 | 1.439 ± 0.065 | 1.425 ± 0.061 |
| | LAYER2 | 2.529 ± 0.066 | 2.147 ± 0.100 | 1.980 ± 0.111 | 1.881 ± 0.100 | 2.318 ± 0.043 | 1.860 ± 0.082 | 1.584 ± 0.090 | 1.561 ± 0.083 |
| | LAYER3 | 2.400 ± 0.051 | 2.171 ± 0.051 | 2.064 ± 0.075 | 2.000 ± 0.066 | 2.315 ± 0.060 | 1.894 ± 0.076 | 1.720 ± 0.082 | 1.664 ± 0.074 |
| RESNET50 ROBUST | LAYER1 | 2.044 ± 0.099 | 1.702 ± 0.117 | 1.539 ± 0.155 | 1.493 ± 0.149 | 1.934 ± 0.051 | 1.397 ± 0.076 | 1.108 ± 0.084 | 1.095 ± 0.077 |
| | LAYER2 | 2.209 ± 0.077 | 1.815 ± 0.105 | 1.678 ± 0.115 | 1.600 ± 0.104 | 2.095 ± 0.045 | 1.502 ± 0.071 | 1.252 ± 0.072 | 1.218 ± 0.065 |
| | LAYER3 | 2.360 ± 0.046 | 1.986 ± 0.070 | 1.824 ± 0.078 | 1.776 ± 0.069 | 2.347 ± 0.067 | 1.713 ± 0.073 | 1.507 ± 0.074 | 1.468 ± 0.067 |
| RESNET18 CAMELYON16 | LAYER1 | 2.511 ± 0.041 | 1.917 ± 0.079 | 1.718 ± 0.081 | 1.671 ± 0.076 | 2.254 ± 0.038 | 1.531 ± 0.061 | 1.146 ± 0.060 | 1.105 ± 0.054 |
| | LAYER2 | 2.328 ± 0.054 | 1.884 ± 0.081 | 1.723 ± 0.076 | 1.671 ± 0.074 | 1.988 ± 0.060 | 1.361 ± 0.056 | 1.030 ± 0.050 | 1.005 ± 0.047 |
| | LAYER3 | 2.170 ± 0.050 | 1.620 ± 0.050 | 1.516 ± 0.046 | 1.433 ± 0.054 | 2.189 ± 0.063 | 1.296 ± 0.042 | 1.048 ± 0.034 | 1.001 ± 0.034 |
| RESNET34 DIGIPATH | LAYER1 | 2.864 ± 0.023 | 1.965 ± 0.120 | 1.644 ± 0.179 | 1.640 ± 0.195 | 2.713 ± 0.031 | 1.741 ± 0.042 | 1.177 ± 0.045 | 1.120 ± 0.044 |
| | LAYER2 | 2.642 ± 0.040 | 1.811 ± 0.212 | 1.601 ± 0.210 | 1.508 ± 0.205 | 2.391 ± 0.062 | 1.357 ± 0.119 | 0.902 ± 0.096 | 0.880 ± 0.100 |
| | LAYER3 | 2.395 ± 0.055 | 1.249 ± 0.136 | 1.080 ± 0.129 | 1.031 ± 0.114 | 2.444 ± 0.060 | 1.026 ± 0.092 | 0.704 ± 0.069 | 0.698 ± 0.059 |

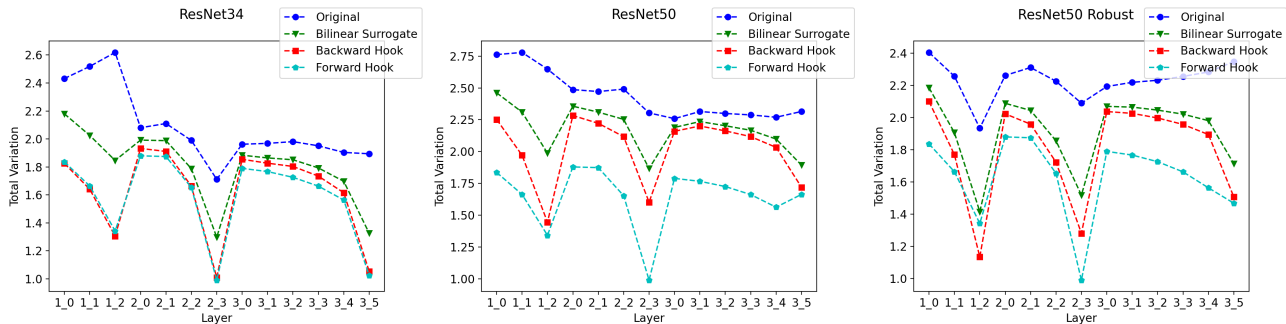


Figure 4. Total variation of the gradient saliency map method.

after the max pool (at two downsamplings away from the input) till the layer before the lowest resolution stage. We do not evaluate earlier layers since we want to compute saliency towards deeper layers. And we do not evaluate layers at the lowest resolution stage since there is no convolutional downsampling coming after them, and therefore no checkerboard noise in the gradient. Layer1, Layer2 and Layer3 from Table 4 correspond to 1.2, 2.3 respectively 3.5 in Figure 4. We observe a reduction in TV for our bilinear surrogate models compared to the original models through all layers. The backward hook method has slightly lower TV compared to the bilinear surrogate method, and the forward hook method has the lowest TV.

4.2.3. CASE STUDIES

In this section we look at and discuss some example images. The saliency maps have the spatial resolution of the layer they have been computed at, which is lower than the input resolution. Therefore we upscale them to the size of the input.

An example for the usefulness of using saliency maps in hidden layers, is shown in Figure 7 and Figure 8. Figure 7 shows the saliency map for a single input image, for both

the original model (bottom two rows) and the bilinear surrogate model (top two rows) for the input layer, Layer1, Layer2, Layer3, Layer4 (from left to right). The top of the two rows is the saliency map, the bottom is overlaying it with the input image. The saliency map for the input layer is highlighting edges and noise, and does not give much information about which structures the network uses to make its prediction. Similarly, the saliency map for Layer4, which is the last convolutional layer (in the encoder of the model), is also not very helpful here, because it is just highlighting the whole tumor. Since the model is a semantic segmentation network, this does not add more information than the prediction already gives.

The saliency map for the hidden layers for the bilinear surrogate model does add additional information though. In Layer1, we can see individual cell nuclei being highlighted, telling us which kind of cells the model is using to support its prediction. In Layer2, and Layer3 we can see structures formed by the cell nuclei.

Figure 8 only shows the center 512x512 pixels of the 1536x1536 images of Figure 7 for the input layer and Layer1. There we can see the highlighted cell nuclei more clearly.

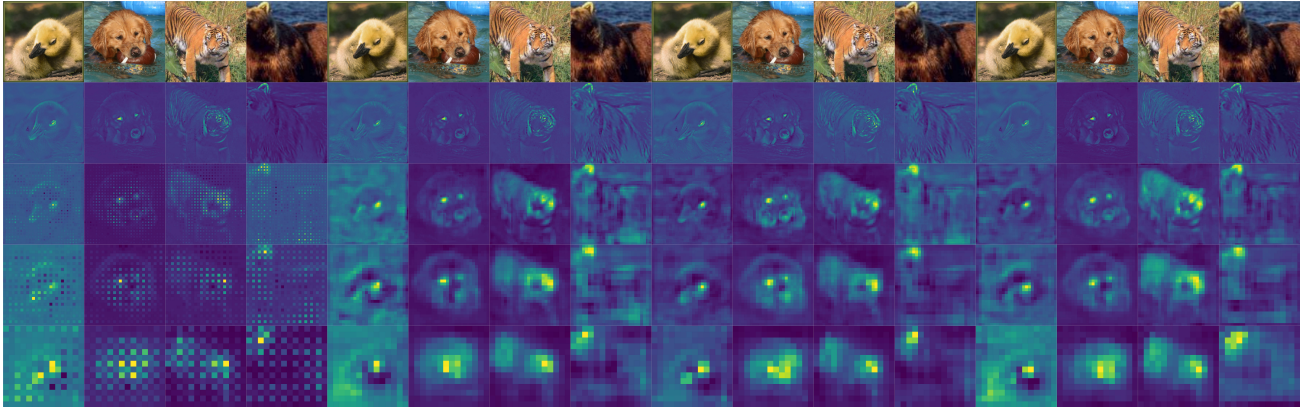


Figure 5. Saliency map from DeepLift from original model (first 4 images from the left), bilinear surrogate model (second 4 images from the left), backward hooked model (third 4 images) and forward hooked model (last 4 images). For the robust ResNet50. From top to bottom shows the original input image, saliency map for the input layer, Layer1, Layer2, Layer3.

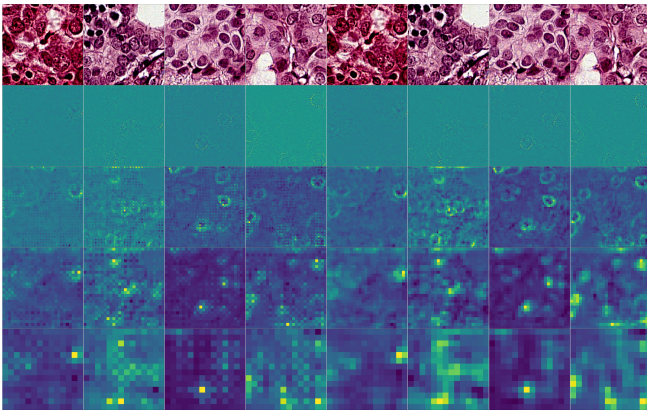


Figure 6. Saliency map from DeepLift from original (left 4 images), and bilinear surrogate model (right 4 images). For a ResNet18 on Camelyon16 data.

Figure 5 shows saliency maps for the robust ResNet50. From left to right in pairs of 4 images it shows the saliency maps for the original model, the bilinear surrogate model, the backward hooked model and the forward hooked model. From top to bottom it shows the original input, saliency map for the input, Layer1, Layer2 and Layer3. The saliency map at the input is smooth in all cases. But for the deeper layers there is a strong checkerboard noise pattern for the original model, whereas the maps for the other methods (bilinear surrogate, backward hooked model, forward hooked model) are smooth.

Something similar can be observed for Figure 6. The figure shows saliency maps for the ResNet18 Camelyon16 for the original (left 4 images) and bilinear surrogate model (right 4 images) for Camelyon16 samples. From top to bottom it shows the input image, saliency map for the input, for Layer1, Layer2, Layer3. The model classified all 4 images

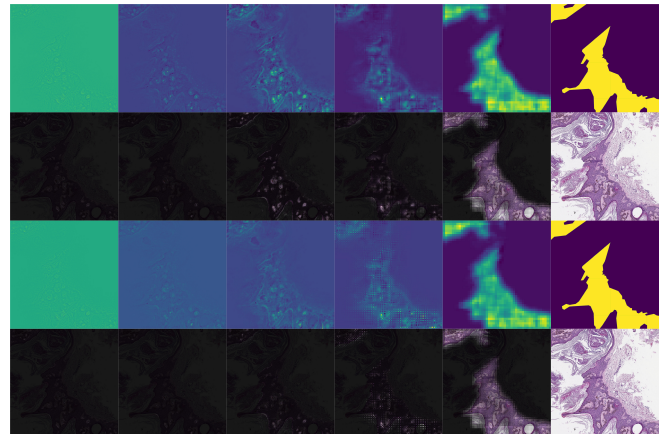


Figure 7. Saliency map from DeepLift for the ResNet34 on Digi-path data. From left to right is: For the input layer, for Layer1, Layer2, Layer3, Layer4, ground truth tumor mask and input image. The top two rows are for the bilinear surrogate model, the bottom two rows are for the original model.

as tumor. The input layer is noisy and difficult to interpret. In the deeper layers, the original model exhibits checkerboard noise in its saliency maps, whereas the saliency maps for the bilinear surrogate model are smoother and easier to interpret. In Layer1 we can see cell nuclei being outlined, whereas deeper in Layer2 we can see the segmentations of whole cell nuclei.

4.3. Additional Discussion

While the forward hook method has the lowest TV, and therefore smoothest saliency maps, it has considerably lower accuracy compared to the original model and its predictions differ rather strongly. The bilinear surrogate method closely matches the accuracy of the original model, while consid-

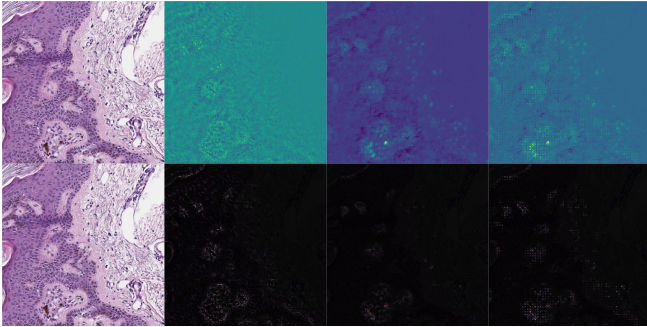


Figure 8. Saliency map from DeepLift on Digipath data, zoomed in on Figure 7. From left to right is: Input image, saliency map for the original model in the input layer, saliency map of the surrogate model for Layer1, saliency map of the original model for Layer1.

erably reducing the TV and the checkerboard noise. The backward hook method also considerably reduces the TV and needs no training of a surrogate model, but here it is unclear how faithful the saliency map is to the original model.

5. Limitations

For the bilinear surrogate method to work, we need access to training data, in order to train the surrogate model. Further, since all our methods reduce noise coming from convolutional downsampling, they are only applicable for models that utilize convolutional downsampling. And since we are not computing the saliency map in the input but in a hidden layer and then overlay it with the input, we assume that the activations in hidden layers are localized (i.e. what the model extracts in a hidden layer and what we see in the input at those spots is roughly the same).

6. Conclusion and Future Work

We successfully investigated three methods to remove checkerboard noise of saliency maps in hidden layers of models that utilize convolutional downsampling. The bilinear surrogate method closely matches the accuracy and predictions of the original model, while reducing the noise in the saliency map, measured by TV. We observed a reduction in TV through all measured layers. While the forward hook method also removes the checkerboard noise, it has a lower accuracy and its predictions differ more strongly from the original model. Overall we recommend first trying the backward hook method, which removes the checkerboard noise and requires no additional training, then if the saliency map from hidden layers gives useful results, train a bilinear surrogate model.

For future work, it would be interesting to check whether we can use the explanations gained from the bilinear surrogate model to explain the original model, but more experiments

specifically to validate this would be needed.

7. Impact Statement

This paper presents work whose goal is to improve transparency of machine learning models. Apart from the many potential societal consequences of generally advancing the field of machine learning, improving transparency of the models can help with their acceptance in a broad sense.

8. Acknowledgements

R.H. is funded by the Deutsche Forschungsgemeinschaft (DFG, German Research Foundation) - project number 459360854. M. S. and D. O. B. acknowledge the financial support by the German Federal Ministry for Economic Affairs and Climate Action (BMWK) and the European Social Fund (ESF) within the EXIST transfer of research project "aisencia" and the financial support by the Federal Ministry of Education and Research (BMBF) within the T!Raum project "MOIN - MUKIDerm".

References

- Deng, J., Dong, W., Socher, R., Li, L., Kai Li, and Li Fei-Fei. ImageNet: A large-scale hierarchical image database. In *2009 IEEE Conference on Computer Vision and Pattern Recognition*, pp. 248–255, 2009. doi: 10.1109/CVPR.2009.5206848.
- Ehteshami Bejnordi, B., Veta, M., Johannes van Diest, P., van Ginneken, B., Karssemeijer, N., Litjens, G., van der Laak, J. A. W. M., the CAMELYON16 Consortium, Hermesen, M., Manson, Q. F., Balkenhol, M., Geessink, O., Stathonikos, N., van Dijk, M. C., Bult, P., Beca, F., Beck, A. H., Wang, D., Khosla, A., Gargeya, R., Irshad, H., Zhong, A., Dou, Q., Li, Q., Chen, H., Lin, H.-J., Heng, P.-A., Haß, C., Bruni, E., Wong, Q., Halici, U., Öner, M. Ü., Cetin-Atalay, R., Berseth, M., Khvatkov, V., Vylegzhanin, A., Kraus, O., Shaban, M., Rajpoot, N., Awan, R., Sirinukunwattana, K., Qaiser, T., Tsang, Y.-W., Tellez, D., Annuschein, J., Hufnagl, P., Valkonen, M., Kartasalo, K., Latonen, L., Ruusuvaori, P., Liimatainen, K., Albarqouni, S., Mungal, B., George, A., Demirci, S., Navab, N., Watanabe, S., Seno, S., Takenaka, Y., Matsuda, H., Ahmady Phoulady, H., Kovalev, V., Kalinovskiy, A., Liauchuk, V., Bueno, G., Fernandez-Carrobles, M. M., Serrano, I., Deniz, O., Racoceanu, D., and Venâncio, R. Diagnostic assessment of deep learning algorithms for detection of lymph node metastases in women with breast cancer. *JAMA*, 318(22):2199–2210, December 2017.
- He, K., Zhang, X., Ren, S., and Sun, J. Deep residual learning for image recognition. In *2016 IEEE Conference*

- on *Computer Vision and Pattern Recognition (CVPR)*, pp. 770–778, 2016. doi: 10.1109/CVPR.2016.90.
- Kingma, D. P. and Ba, J. Adam: A Method for Stochastic Optimization. In *3rd International Conference on Learning Representations, ICLR 2015, San Diego, CA, USA, May 7-9, 2015, Conference Track Proceedings*, 2015.
- Kokhlikyan, N., Miglani, V., Martin, M., Wang, E., Al-sallakh, B., Reynolds, J., Melnikov, A., Kliushkina, N., Araya, C., Yan, S., and Reblitz-Richardson, O. Captum: A unified and generic model interpretability library for pytorch, 2020.
- Odena, A., Dumoulin, V., and Olah, C. Deconvolution and checkerboard artifacts. *Distill*, 2016. doi: 10.23915/distill.00003. URL <http://distill.pub/2016/deconv-checkerboard>.
- Olah, C., Mordvintsev, A., and Schubert, L. Feature visualization. *Distill*, 2017. doi: 10.23915/distill.00007. <https://distill.pub/2017/feature-visualization>.
- Olah, C., Satyanarayan, A., Johnson, I., Carter, S., Schubert, L., Ye, K., and Mordvintsev, A. The building blocks of interpretability. *Distill*, 2018. doi: 10.23915/distill.00010. <https://distill.pub/2018/building-blocks>.
- Oquab, M., Bottou, L., Laptev, I., and Sivic, J. Is object localization for free? - weakly-supervised learning with convolutional neural networks. In *Proceedings of the IEEE Conference on Computer Vision and Pattern Recognition (CVPR)*, June 2015.
- Paszke, A., Gross, S., Massa, F., Lerer, A., Bradbury, J., Chanan, G., Killeen, T., Lin, Z., Gimelshein, N., Antiga, L., Desmaison, A., Köpf, A., Yang, E. Z., DeVito, Z., Raison, M., Tejani, A., Chilamkurthy, S., Steiner, B., Fang, L., Bai, J., and Chintala, S. Pytorch: An imperative style, high-performance deep learning library. In Wallach, H. M., Larochelle, H., Beygelzimer, A., d’Alché-Buc, F., Fox, E. B., and Garnett, R. (eds.), *Advances in Neural Information Processing Systems 32: Annual Conference on Neural Information Processing Systems 2019, NeurIPS 2019, December 8-14, 2019, Vancouver, BC, Canada*, pp. 8024–8035, 2019. URL <https://proceedings.neurips.cc/paper/2019/hash/bdbca288fee7f92f2bfa9f7012727740-Abstract.html>.
- Petsiuk, V., Das, A., and Saenko, K. Rise: Randomized input sampling for explanation of black-box models, 2018.
- Rao, S., Böhle, M., and Schiele, B. Towards better understanding attribution methods. In *Proceedings of the IEEE/CVF Conference on Computer Vision and Pattern Recognition (CVPR)*, pp. 10223–10232, June 2022.
- Santurkar, S., Ilyas, A., Tsipras, D., Engstrom, L., Tran, B., and Madry, A. Image synthesis with a single (robust) classifier. In Wallach, H., Larochelle, H., Beygelzimer, A., d’Alché-Buc, F., Fox, E., and Garnett, R. (eds.), *Advances in Neural Information Processing Systems*, volume 32. Curran Associates, Inc., 2019. URL https://proceedings.neurips.cc/paper_files/paper/2019/file/6f2268bd1d3d3ebaabb04d6b5d099425-Paper.pdf.
- Selvaraju, R. R., Cogswell, M., Das, A., Vedantam, R., Parikh, D., and Batra, D. Grad-cam: Visual explanations from deep networks via gradient-based localization. In *Proceedings of the IEEE International Conference on Computer Vision (ICCV)*, Oct 2017.
- Shrikumar, A., Greenside, P., and Kundaje, A. Learning important features through propagating activation differences, 2019.
- Simonyan, K., Vedaldi, A., and Zisserman, A. Deep inside convolutional networks: Visualising image classification models and saliency maps, 2014.
- Smilkov, D., Thorat, N., Kim, B., Viégas, F., and Wattenberg, M. Smoothgrad: removing noise by adding noise, 2017. URL <https://arxiv.org/abs/1706.03825>.
- Sundararajan, M., Taly, A., and Yan, Q. Axiomatic attribution for deep networks. In Precup, D. and Teh, Y. W. (eds.), *Proceedings of the 34th International Conference on Machine Learning*, volume 70 of *Proceedings of Machine Learning Research*, pp. 3319–3328. PMLR, 06–11 Aug 2017. URL <https://proceedings.mlr.press/v70/sundararajan17a.html>.